frontiers | Frontiers in Physics

TYPE Original Research
PUBLISHED 10 March 2025
DOI 10.3389/fphy.2025.1484460

OPEN ACCESS

EDITED BY
Ignazio Bombaci,
University of Pisa, Italy

REVIEWED BY
Andres Arazi,
National Atomic Energy Commission, Argentina
Shashi K. Dhiman,
Himachal Pradesh University, India
Parada Tobel Paraduan Hutauruk,
Pukyong National University,
Republic of Korea

*CORRESPONDENCE
Abdul Kabir,
kabirkhanak1@gmail.com

RECEIVED 21 August 2024
ACCEPTED 08 January 2025
PUBLISHED 10 March 2025

CITATION
Kabir A, Nabi J-U, Almujibah H, Anwaar I and Raza N-UA (2025) Re-examining the impact of ^{63}Co and ^{63}Ni in the stellar environment. *Front. Phys.* 13:1484460.
doi: 10.3389/fphy.2025.1484460

Re-examining the impact of ^{63}Co and ^{63}Ni in the stellar environment

Abdul Kabir[1]*, Jameel-Un Nabi[2], Hamad Almujibah[3], Izzah Anwaar[1] and Noor-Ul Ain Raza[1]

[1]Space and Astrophysics Research Lab, National Centre of GIS and SpaceApplications, Department of Space Science, Institute of Space Technology, Islamabad, Pakistan, [2]University of Wah, Wah Cantonment, Punjab, Pakistan, [3]Department of Civil Engineering, College of Engineering, Taif University, Ta'if, Saudi Arabia

The nuclear ground state properties of ^{63}Co and ^{63}Ni nuclei have been investigated within the framework of the relativistic mean field (RMF) approach. The RMF model with density-dependent meson-exchange (DD-ME2) interaction is used to calculate the potential energy curves (PECs) and nuclear ground state deformation parameters (β_2) of ^{63}Co and ^{63}Ni. The blocking effects of the unpaired nucleon are considered using the equal filling approach for the odd-A system. Later, the β-decay properties, including the stellar weak rates and Gamow–Teller (GT) strength of ^{63}Co and ^{63}Ni, are studied using the proton-neutron quasiparticle random-phase approximation (pn-QRPA) model. The β_2 values computed from the RMF model are employed in the pn-QRPA framework as an input parameter for the calculations of β-decay properties for ^{63}Co and ^{63}Ni. The stellar rates are compared with the projected shell model (PSM) results. For all densities, the pn-QRPA rates are found to be higher than the stellar rates computed via the PSM to a factor of 1.3 or more. The findings reported in the present investigation might be useful for simulating the late-stage stellar evolution of massive stars and the *s*-process of nucleosynthesis.

KEYWORDS

pn-QRPA, β-decay properties, GT strength distribution, deformation parameter, RMF model, stellar rates

1 Introduction

The rapid neutron-capture process (*r*-process) is the primary nucleosynthesis mechanism responsible for the production of nuclei more massive than iron [1, 2]. The *r*-process often occurs in a stellar exploding scenario with a high neutron density flux. It was noted that at the same astrophysical parameters of constant density and temperature, it is not possible to synthesize all of the nuclear matter simultaneously [3, 4]. Hence, neutron capture proceeds far more quickly than competing beta decay. The larger neutron-flux matter, which has comparably little and roughly constant S_n (neutron separation energy), is followed by the *r*-process route. The *r*-process flow of matter slows at neutron magic shell isotones. The trajectory of the *r*-process and the abundance distribution are significantly influenced by the half-life predictions.

The Gamow–Teller (GT) transition is widely believed to contribute to the stellar rates [5]. GT distributions have been produced experimentally using various approaches [6, 7]. The GT strength may be measured by charge-exchange reactions for nuclei in or close to the beta stability valley under terrestrial conditions when the parent nuclei stay in their ground states [8]. Several nuclei located beyond the beta stability valley play a crucial role in various astrophysical processes, including the *r*-process, the *rp*-process, and neutron star cooling. In extremely hot and dense stellar scenarios, nuclei may become thermally populated in their excited states. Existing study techniques are still insufficient to conduct a thorough investigation into the GT strength of nuclei beyond the beta stability valley or when the parent nuclei exist in their excited states.

Weak interactions between finite nuclei hold significance in various disciplines, including particle physics and nuclear astrophysics [9–11]. Reliable weak-interaction rates of finite nuclei in high temperatures and high-densities stellar scenarios are crucial for understanding astrophysical challenges like stellar advancement and the origins of heavy elements. There are three different sorts of implications from stellar weak-interaction processes: converting neutrons to protons, reducing the density of positrons or electrons inside the stellar environment, and neutrino emissions [12–17]. Understanding the core-collapse supernova is therefore dependent on the stellar weak rates [18], the *s*-process (slow neutron-capture process) [19, 20], the *r*-process (rapid neutron-capture process) [21], and the *rp*– process (rapid proton-capture process) [22].

The GT strength and the weak-interaction rates have been studied theoretically using a variety of nuclear structure models that have been developed over the past few decades. Fuller, Fowler, and Newman (FFN) accomplished groundbreaking work for the systematic calculation of nuclear stellar weak-interaction rates [12–14]. For the analysis of GT transition and stellar weak-interaction rate, the most dependable approach in current practice is the shell model (SM), which has a full diagonalization of an effective Hamiltonian in a selected model space [23]. Additional methods are anticipated for the GT strength and stellar weak rates in applications, such as the hybrid model based on the shell model Monte Carlo approach and the random-phase approximation (RPA) [24], the quasiparticle random-phase approximation (QRPA) [25], and the most recent traditional projected shell model (PSM) [26, 27].

Massive stars have an onion-like structure prior to the supernova stage, where the Fe, Co, and Ni mass-region nuclei play crucial roles in the core. Depending on neutron excess, nuclear beta decays and electron captures compete before the core collapses [28]. However, it is anticipated that most heavy nuclei close to or inside the beta stability valley originated from the *s*-process. ^{63}Ni is a potential candidate for the *s*-process and similarly, ^{63}Co is a potential candidate in the pre-supernova collapse stage.

In the present work, we employed the RMF approach with density-dependent meson-exchange interactions to examine the nuclear ground state properties, including the binding energies and β_2 related to $A = 63$ (^{63}Co and ^{63}Ni). We analyzed the potential energy curves (PECs) that are important for the extraction of β_2. For the analysis of GT strength and stellar weak rates of ^{63}Co and ^{63}Ni, we utilized the pn-QRPA approach. We revised the calculations based on our present recipes to investigate beta decay properties. For example, our first aim is to extract the ground state deformation parameter (β_2) from the minima of relative energy curves computed via the RMF framework. Then, we will check the potential effects of β_2 on the GT strength distributions and stellar weak rates for ^{63}Co and ^{63}Ni. The present model-based analysis is compared with previously observed and predicted data.

The paper is organized as follows. In Section 2, we provide a brief explanation of the RMF and pn-QRPA models used to calculate the nuclear structure and β-decay properties, respectively. Section 3 presents our results with relevant discussion. Section 4 concludes the findings of the current investigation.

2 Theoretical framework

2.1 The RMF model

The RMF model is a theoretical tool used for the description of nuclear structure properties of nuclei (see [29] and related references). The preliminary model [30] struggled to describe nuclear surface features and the incompressibility of nuclear matter. To address this, a nonlinear model was developed [29]. The later versions of the model were termed covariant density functional theory and included a density-dependent meson-exchange model [31]. In the present investigation, the ground state parameters for nuclei have been determined by employing the density-dependent meson-exchange (DD-ME2) [32] version of the RMF framework. According to the RMF model, nucleons interact by exchanging various mesons and photons [30]. The first version of the RMF model ran into several issues while attempting to describe the incompressibility of nuclear matter and the surface characteristics of nuclei. This led to the introduction of the model's nonlinear variant [29]. Subsequent versions of the RMF framework, known as covariant density functional theory, developed with elements including point coupling (PC) and meson-exchange (ME) [31, 33, 34]. We utilized the density-dependent -(ME) framework in our analysis. The density-dependent meson-exchange variant of the RMF model considers the isoscalar scalar σ meson, the isoscalar vector ω meson, and the isovector vector ρ meson fields for the analysis of nuclear matter and single-particle nuclear properties. In the DD-ME model, the coupling constants are self-consistently governed by nuclear functions. The definition of the Lagrangian density is given below.

$$\begin{aligned}\mathcal{L}_{DDME} = \bar{\psi}\Big[\gamma_\mu\left(i\partial^\mu - \Gamma_\omega\omega^\mu - \Gamma_\rho\tau\cdot\rho_\mu\right) - \left(M - \Gamma_\sigma\sigma\right)\\ - e\gamma^\mu A_\mu\frac{1-\tau_3}{2}\Big]\psi - \frac{1}{2}\left(\partial^\mu\sigma\partial_\mu\sigma - m_\sigma^2\sigma^2\right)\\ -\frac{1}{4}\Omega^{\mu\nu}\Omega_{\mu\nu} + \frac{1}{2}m_\omega^2\omega^\mu\omega_\mu - \frac{1}{4}\vec{R}^{\mu\nu}\cdot\vec{R}\mu\nu\\ +\frac{1}{2}m_\rho^2\vec{\rho}^\mu\cdot\vec{\rho}_\mu - \frac{1}{4}F^{\mu\nu}\cdot F_{\mu\nu}.\end{aligned} \tag{1}$$

In Equation 1, the terms Γ_σ, Γ_ω, and Γ_ρ depend on the (nucleon) density, which is further defined by Equation 2:

$$\Gamma_i(\rho) = \Gamma_i(\rho_{sat})\, f_i(x), \tag{2}$$

where i is generalized for the ρ, ω, and σ, respectively. Similarly, x is the ratio of ρ_b (density of baryon), and ρ_{sat} (density of baryon at saturation). $f(x)$ is defined for the σ or ω meson by Equation 3:

$$f_j(x) = a_j\frac{1 + b_j\left(x + d_j\right)^2}{1 + c_j\left(x + d_j\right)^2}, \quad j = \omega, \quad \sigma \tag{3}$$

whereas for the ρ meson, $f(x)$ is defined by Equation 4:

$$f_\rho(x) = e^{-a_\rho(x-1)}. \tag{4}$$

The DD-ME2 interactions ([35–38]) are often employed as covariant density functionals in the DD-ME model.

Studying even-even systems within the mean field approach is a good approximation. In this case, the configurations, neglected above the mean field ground state, are 4- or higher-quasiparticle (qp) configurations. The 2-qp configurations do not couple to the Hamiltonian ($H_{20} = 0$). Mixing configurations are relatively few and separated by the pairing gaps. The exact solution has only a small admixture of higher qp configurations (4-qp and higher). On the other hand, investigating odd-A nuclei using the RMF model is rather challenging. In this case, there are many 3-qp states in the region close to the ground state, which may mix. The pairing gap even increases the level density of neighboring 1-qp states. Only a few of the H_{31} matrix elements vanish. The mean field approximation in odd-A cases is not as good as in even-even nuclei. Of course, sometimes symmetries help (K-value in deformed nuclei), but this is not always the case. We performed the HFB calculations in odd-A systems by using the blocking technique. The blocking was carried out by replacing one U-vector with the corresponding V-vector (see Section 6.3.2 of [39]). We carried out the blocking calculations with small modifications of the HFB code [40]. Pairing correlations play an important role for open-shell nuclei, and the Bardeen–Cooper–Schrieffer (BCS) approximation was used to tackle these correlations. Furthermore, constant G approximation [41] was used for the PEC calculations.

2.2 The pn-QRPA model

The pn-QRPA model is employed to analyze GT strength distributions and stellar weak rates. The Hamiltonian configuration in the pn-QRPA model may be characterized using Equation 5:

$$\mathcal{H}^{QRPA} = \mathcal{H}^{sp} + \mathcal{V}^{pair} + \mathcal{V}^{pp}_{GT} + \mathcal{V}^{ph}_{GT}. \tag{5}$$

The Hamiltonian for a single particle is denoted as $\mathcal{H}^{sp}$, while $\mathcal{V}^{\mathrm{pair}}$ represents the interaction between nucleons. The terms $\mathcal{V}^{pp}_{GT}$ and $\mathcal{V}^{ph}_{GT}$ correspond to interactions involving particle-particle (pp) and particle-hole (ph) GT interactions, respectively. Wave functions and energies of individual particles are calculated via the Nilsson model [42]. The oscillator constant is determined using $\hbar\omega = \left(45 \quad \boldsymbol{A}^{-1/3} - 25 \quad \boldsymbol{A}^{-2/3}\right)$. Other crucial factors affecting weak-interaction rates consist of β_2, the nucleon pairing gap ($\Delta_{nucleon}$), parameters of the Nilsson potential (PNP), and the Q-values. The PNP parameters were sourced from [43], and Q-values were derived through the calculation of mass excess values as presented in the compilation [44]. In order to obtain proton and neutron quasiparticle energies and occupation probabilities, the BCS equations were solved with pairing gaps computed using Equations 6, 7:

$$\Delta_{nn} = \frac{1}{8}(-1)^{A-Z+1}\left[2S_n(A+1,Z) - 4S_n(A,Z) + 2S_n(A-1,Z)\right], \tag{6}$$

$$\Delta_{pp} = \frac{1}{8}(-1)^{1+Z}\left[2S_p(A+1,Z+1) - 4S_p(A,Z) + 2S_p(A-1,Z-1)\right], \tag{7}$$

where S_p (S_n) is the separation energy of protons and neutrons, respectively. As mentioned earlier, the β_2 values were determined using the RMF model. β_2 is determined by using Equation 8:

$$\beta_2 = \frac{125 Q_2}{1.44 A^{2/3} Z}, \tag{8}$$

where Q_2 denotes the electric quadrupole moment chosen from [45] or the RMF framework. In the pn-QRPA model, the charge-changing reaction transitions are defined by phonon creation operators. The pn-QRPA phonons are given as Equation 9:

$$A^+_\omega(\mu) = \sum_{pn}\left(X^{pn}_\omega(\mu)\, a^+_p a^+_{\bar{n}} - Y^{pn}_\omega(\mu)\, a_n a_{\bar{p}}\right). \tag{9}$$

Here, the summation is taken on all the p-n pairs having $\mu = m_p - M_n = 0, \pm 1$, and $m_n(m_p)$ represents the angular momentum third component of the neutron (proton). The operators $a^+_{n(p)}$ signify the creation of a quasiparticle (q.p) state for either a neutron or a proton, and $\bar{p}$ represents the time-reversed state of p. In the context of QRPA phonons, the theory defines the ground state as the vacuum, symbolized by $\mathrm{A}_\omega(\mu)|QRPA\rangle = 0$. The phonon operator's excitation energy (ω) and amplitudes (X_ω, Y_ω) are acquired by solving Equation 10, which is the well-known RPA equation.

$$\begin{bmatrix} C & D \\ -D & -C \end{bmatrix}\begin{bmatrix} X \\ Y \end{bmatrix} = \omega \begin{bmatrix} X \\ Y \end{bmatrix}, \tag{10}$$

Here, $X(Y)$ represent forward (backward) amplitudes. The ω shows the energy eigenvalues of the eigenfunctions, and the two sub-matrices are specified by Equations 11, 12:

$$C_{pn,p'n'} = V^{pp}_{pn,p'n'}\left(u_p u_n u_{p'} u_{n'} + v_p v_n v_{p'} v_{n'}\right) + V^{ph}_{pn',p'n'}\left(u_p v_n u_{p'} u_{n'} + v_p u_n v_{p'} v_{n'}\right) + \delta(pn,p'n')\left(\varepsilon_n + \varepsilon_p\right), \tag{11}$$

$$D_{pn,p'n'} = +V^{pp}_{pn,p'n'}\left(u_p u_n v_{p'} v_{n'} + v_p v_n u_{p'} u_{n'}\right) - V^{ph}_{pn,p'n'}\left(u_p v_n v_{p'} u_{n'} + v_p u_n u_{p'} v_{n'}\right). \tag{12}$$

Here, the $\varepsilon_{n(p)}$ shows the q.p energies of the neutron (proton), whereas $\mathrm{v}_{p(n)}$ and $\mathrm{u}_{p(n)}$ represent the occupation and unoccupation amplitudes and are treated in the BCS theory. The detailed solution of the RPA matrix equation can be seen in [46]. The pairing force is calculated using the BCS approximation. These calculations were performed separately for both proton and neutron. We took a constant pairing force of strength G (G_p and G_n for protons and neutrons, respectively),

$$\mathcal{V}_{pair} = -G \sum_{jkj'k'} (-1)^{l+j-k} s^\dagger_{jk} s^\dagger_{j-k} \times (-1)^{l'+j'-k'} s_{j'-k'} s_{j'k'}, \tag{13}$$

where l is orbital angular momentum, and summation over k and k' is restricted to positive values. The proton-neutron residual interactions take place through the pp and ph GT forces, which were characterized by interaction constants κ and χ, respectively, in the pn-QRPA framework. The pp GT force is explained using Equations 14, 15:

$$\mathcal{V}^{pp}_{GT} = -2\kappa \sum_{\mu=-1}^{1} (-1)^\mu \mathcal{O}^\dagger_\mu \mathcal{O}_{-\mu}, \tag{14}$$

with

$$\mathcal{O}^\dagger_\mu = \sum_{j_p k_p j_n k_n} < j_n k_n \mid \left(t_\pm \sigma_\mu\right)^\dagger \mid j_p k_p > \times (-1)^{l_n + j_n - k_n} s^\dagger_{j_p k_p} s^\dagger_{j_n - k_n}. \tag{15}$$

In order to calculate the *ph* GT force, we used Equations 16, 17:

$$\mathcal{V}^{ph}_{GT} = +2\chi \sum_{\mu=-1}^{1} (-1)^{\mu} \mathcal{U}_{\mu} \mathcal{U}^{\dagger}_{-\mu}, \tag{16}$$

with

$$\mathcal{U}_{\mu} = \sum_{j_p k_p j_n k_n} < j_p k_p \mid t_{\pm} \sigma_{\mu} \mid j_n k_n > s^{\dagger}_{j_p k_p} s_{j_n k_n}. \tag{17}$$

The κ and χ interaction strengths were determined using the relation $0.58/A^{0.7}$ and $5.2/A^{0.7}$, respectively, taken from [47]. Our results fulfilled the model-independent Ikeda sum rule [48]. The reduced GT transition probabilities were calculated using Equation 18:

$$B_{GT}(\omega) = |\langle \omega, \mu \| \tau_{\pm} \sigma_{\mu} \| QRPA \rangle|^2, \tag{18}$$

where σ_{μ} is the spin operator, and $\tau_{\pm} = \tau_x \pm \iota \tau_y$ are the isospin raising and lowering operators, respectively. The model-independent Ikeda sum rule may be evaluated using Equation 19 for the operators:

$$S_{-} + S_{+} = \sum_{f} |\langle f|\hat{O}_{-}|i\rangle|^2 + \sum_{f} |\langle f|\hat{O}_{+}|i\rangle|^2 = 3(N-Z), \tag{19}$$

where $|i\rangle$ represents the parent state, and $|f\rangle$ represents the daughter state connected via the GT operator. For further details, see [49–51].

The stellar β-decay (we subsequently refer to this as electron emission *EE*) and positron capture (*PC*) rates between parent level n and daughter state m have been determined utilizing Equation 20:

$$\lambda^{EE/PC}_{mn} = \ln 2 \frac{f^{EE/PC}_{mn}(\rho, T, E_f)}{(ft)_{mn}}, \tag{20}$$

where $(ft)_{mn}$ corresponds to the GT and Fermi transitions shown in Equations 21–23:

$$B^{mn} = (g_A/g_V)^2 B^{mn}_{GT} + B^{mn}_{F}, \tag{21}$$

$$B^{mn}_{GT} = \frac{1}{2J_m + 1} \langle n \| \sum_k \tau^k_{\pm} \vec{\sigma}^k \| m \rangle|^2, \tag{22}$$

$$B^{mn}_{F} = \frac{1}{2J_m + 1} \langle n \| \sum_k \tau^k_{\pm} \| m \rangle|^2. \tag{23}$$

The construction of low-lying excited levels and computation of nuclear matrix elements in our present analysis may be found in [46]. f_{mn} is the phase space and depends on the core temperature (T), core density (ρ), and Fermi energy (E_f). It was calculated using Equation 24:

$$f^{EE}_{mn} = \int_1^{E_\beta} E_k \sqrt{E_k^2 - 1} \left(E_\beta - E_k\right)^2 F(+Z, E_k)(1 - \mathcal{R}_{-})\, dE_k, \tag{24}$$

for *EE* decay rates. The f_{nm} for *PC* were computed using Equation 25:

$$f^{PC}_{mn} = \int_{E_l}^{\infty} E_k \sqrt{E_k^2 - 1} \left(E_\beta + E_k\right)^2 F(-Z, E_k)\, \mathcal{R}_{+} dE_k, \tag{25}$$

where E_k is the kinetic energy of the electron, and E_l is the total capture threshold energy. The Fermi functions, $F(\pm Z, E_k)$, were calculated using the method described in [52]. The total β decay energy was determined using Equation 26:

$$E_\beta = m_p - m_d + E_m - E_n, \tag{26}$$

where E_n is the excitation energy of the daughter nucleus having mass m_d, while E_m is the corresponding quantities of parent nucleus with mass m_p. The distribution functions have been determined with Equations 27, 28:

$$\mathcal{R}_{-} = \left[\exp\left(\frac{E_k - E_f}{k_\beta T}\right) + 1\right]^{-1}, \tag{27}$$

$$\mathcal{R}_{+} = \left[\exp\left(\frac{E_k + 2 - E_f}{k_\beta T}\right) + 1\right]^{-1}, \tag{28}$$

where k_β is the Boltzmann constant. The electron number density, which is related to nuclei and protons, was determined using Equation 29:

$$\rho Y_e N_A = \frac{1}{\pi^2} \left(\frac{m_e c}{\hbar}\right)^3 \int_0^{\infty} (\mathcal{R}_{-} - \mathcal{R}_{+}) p^2 dp. \tag{29}$$

Here, N_A represents the Avogadro number, Y_e is the ratio of the electron number to the baryon number, and p represents the momentum of positron/electron. The total stellar weak rates were computed using Equation 30:

$$\lambda^{EE/PC} = \sum_{mn} P_m \lambda^{EE/PC}_{mn}, \tag{30}$$

where P_m, which was calculated using the Boltzmann distribution, is the occupancy probability of the parent excited states. We continued to sum the initial and final states until our rate computation reached the necessary degree of convergence.

3 Result and discussion

In the initial phase of our Investigation, we are focusing on the nuclear structure properties of ^{63}Co and ^{63}Ni isobars by utilizing the DD-ME2 interaction parameters within the RMF framework. The odd *A* nuclei are considered in the present investigation utilizing the relativistic Hartree–Bogoliubov (RHB) approach. We consider the blocking effects of the unpaired nucleon, which are included in the equal filling assumption, in order to compute the odd-*A* system. We examined the β_2 for ^{63}Co and ^{63}Ni in detail. To accomplish this, we analyzed the PECs for ^{63}Co and ^{63}Ni within the RMF framework. The constraints on the quadrupole moment are implemented in order to compute binding energy for the analysis of PECs.

In Figure 1, the PECs are expressed as a function of β_2 for ^{63}Co and ^{63}Ni. For the analysis of PECs, the lowest binding energy is used as a reference. The PECs are derived by analyzing the differences between the predicted binding energy for certain β_2 values and the reference binding energy for ^{63}Co and ^{63}Ni. Nuclear shapes are determined by the PEC minima. Prolate nuclei resulted from PEC minima located on the positive value of β_2, whereas for the oblate shape nuclei, the PEC minima are found on the negative values of β_2. In the present investigation, the nuclear shapes in the ground state for ^{63}Co and ^{63}Ni are predicted to be prolate and oblate, respectively. Furthermore, one can see that two energy minima appear on both the prolate and oblate sides of the PECs.

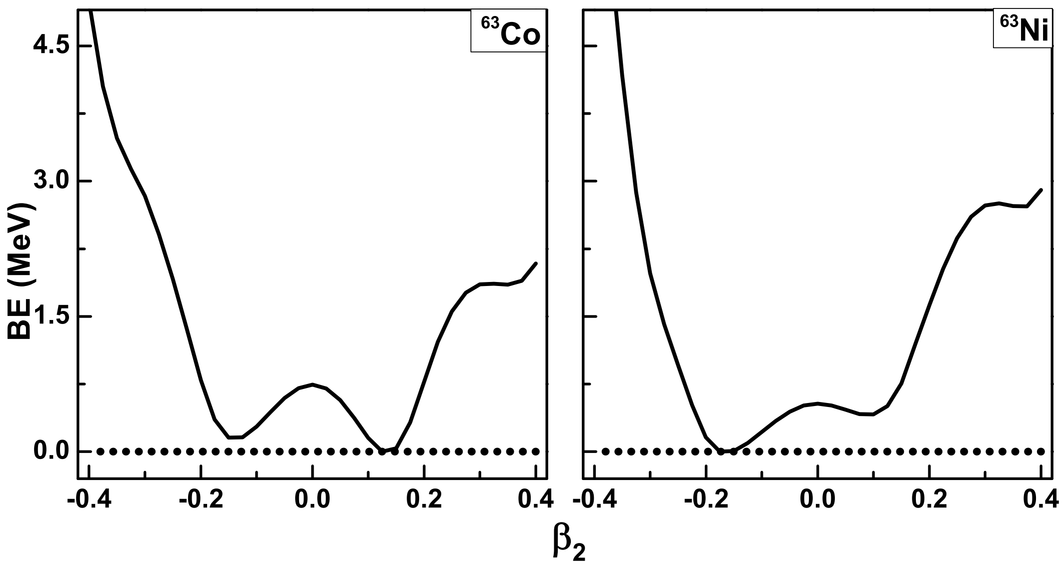

FIGURE 1
Binding energy against the constraint β_2 for ^{63}Co and ^{63}Ni within the RMF framework via DD-ME2 interaction.

The oblate energy minimum for ^{63}Co is more shallow than the prolate energy minimum. Therefore, the prolate shapes have a more probable occurrence in the ground state for ^{63}Co. The oblate minimum existed at excitation energy 0.156 MeV. Similarly, ^{63}Ni has an oblate shape in the ground state; however, it has prolate energy minima that existed at excitation energy 0.412 MeV. In addition to these structural changes, the present analysis predicts a prolate-oblate shape coexistence with a small energy difference, as displayed in Figure 1. The phenomenon of shape coexistence is associated with the occurrence of a low-lying state arising from intruder configurations in addition to the ground state. The β_2 computed via the RMF framework, where the DD-ME2 interaction for the ^{63}Co is 0.188, and the interaction for ^{63}Ni is −0.264. The earlier computed β_2 for ^{63}Co was 0.108 and for ^{63}Ni was 0.107 [45]. They predicted a prolate shape for both nuclei. Similarly, on the website [53], the information related to the PEC is displayed graphically, where ^{63}Co has a prolate shape, and ^{63}Ni has an oblate shape.

The nuclear deformations computed via the RMF model are used as an input parameter in the pn-QRPA model to perform self-consistent calculations of the β-decay properties, including the GT strength and stellar rates of ^{63}Co and ^{63}Ni.

At higher temperatures and densities, ^{63}Co is one of the most important candidates in the core collapse of a massive star. Figure 2 depicts the present model-based computed GT strength along with the measured GT strength [54] and previously computed GT strength based on PSM [27] within the Q-window. It is obvious from Figure 2 that the present computed GT strength agrees well with the results of [54]. The pn-QRPA calculation based on the RMF interactions predicted the strength distribution better than [27]. The splitting of the GT strength into a strong and weak state close to 2.0 MeV fits well with the experimental results. We observe that the present scheme seems able to predict effects due to the fine nuclear structure.

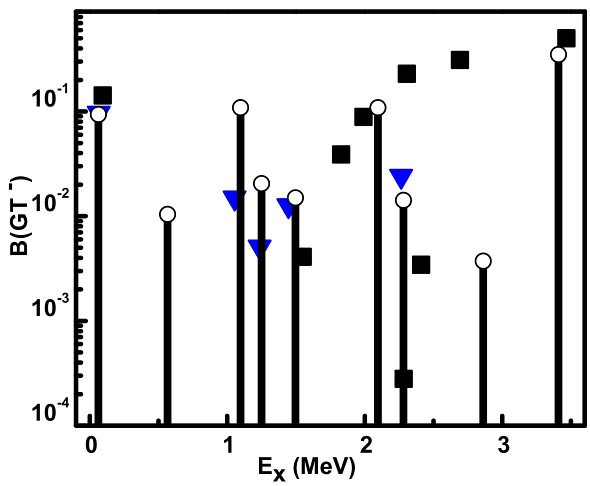

FIGURE 2
GT strength for ^{63}Co via β_2 from the RMF model calculated in the present work (open circles) along with GT strength of [27] (solid squares) and [54] (lower triangles).

The temperature conditions in the stellar environment are so high (in order of 10^9 K) that parent nuclei in excited states have high likelihood of occupancy. This means that the contributions of each excited state to the total weak rates are quantifiable. Consequently, all partial decay rates resulting from distinct parent excited states must be included in the analysis of the microscopic rate. This state-by-state analysis of weak rates is the foundation of the pn-QRPA model. The pn-QRPA model was initially used to determine microscopic weak-interaction rates for a large number of nuclei far from the stability line. The pn-QRPA technique utilizes a mean field basis and potentials, including the Woods–Saxon potential, the Nilsson

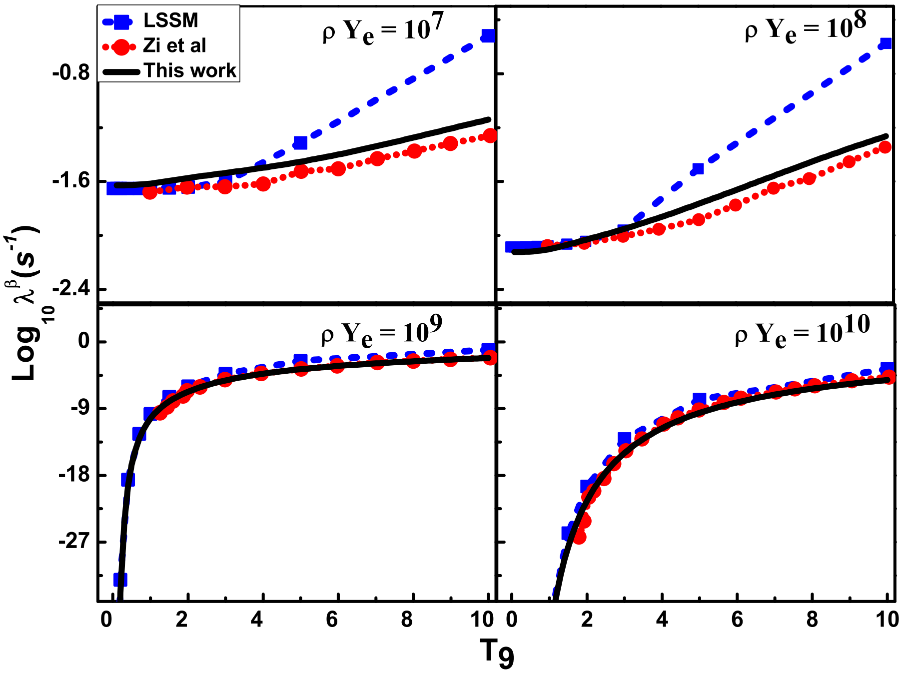

FIGURE 3
Computed stellar β decay rates for ^{63}Co along with the data of Zi et al. [27] and LLSM [5].

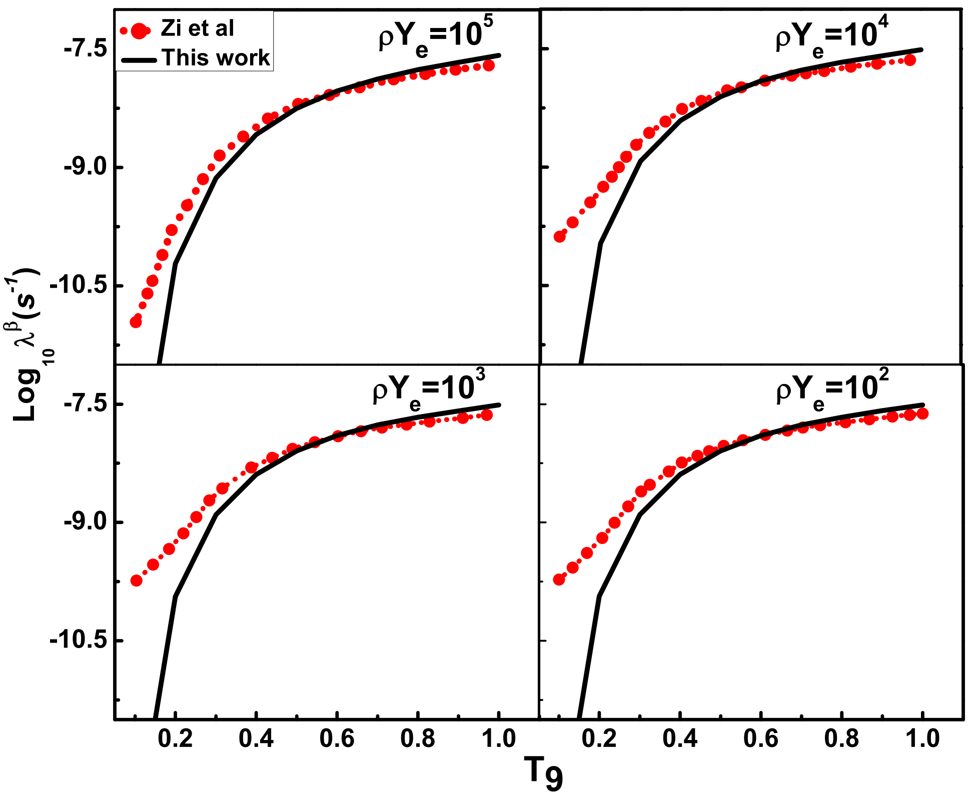

FIGURE 4
Computed stellar β decay rates for ^{63}Ni along with the data of Zi et al. [27].

potential, and the finite-range droplet model. Here, we investigated the β^- rates of ^{63}Co $\rightarrow$ ^{63}Ni at $\rho \quad Y_e = 10^{7-10}$ g cm^{-3}. At high temperatures, the various excited states of the daughter nucleus have a sizeable impact that could additionally contribute to stellar weak decay rates. It is obvious from Figure 3 that at lower densities and high temperatures, the β^- rates are maximum. The present pn-QRPA-based analysis provides larger decay rates than the PSM and smaller decay rates than the results mentioned in [5]. For example, at $\rho Y_e = 10^7$ g cm^{-3} and $T_9 = 10$, the present model-based β^- rates are higher by a factor 1.3 than PSM. Meanwhile, at the same temperature and density, the rates of [5] exceeded the pn-QRPA rates by a factor of 4. Almost the same behavior is followed at $\rho Y_e = 10^8$ g cm^{-3} and $T_9 = 10$. At higher density $\rho Y_e = 10^{10}$ g cm^{-3}, the pn-QRPA rates almost collapse with the PSM and [5] computed rates as mentioned in Figure 3. The GT strength has a dominant impact on the stellar beta decay rates.Furthermore, we analyzed the stellar rates for ^{63}Ni $\rightarrow$ ^{63}Cu in the *s*-process environments at $\rho \quad Y_e = 10^{2-5}$ g cm^{-3} and $T_9 \leq 1$. The present model-based results for rates, along with the predictions of PSM [27], are depicted in Figure 4. We found that at $T_9 \cong 1$, the present pn-QRPA based predictions for rates at all densities ($\rho Y_e = 10^{2-5}$ g cm^{-3}) show good agreement with the rates computed via PSM in [27]. One should note that the stellar weak rates computed at lower temperatures are considerably smaller than rates computed at higher temperatures. The primary factor contributing to the decay rates at low temperatures is the transition between ground states. As the temperature increases, the stellar population probability of the parent nucleus (^{63}Ni) in the ground state decreases while the excited state increases, leading to an increase in the decay rates with the temperature. The stellar weak-interaction rates for both nuclei, that is, ^{63}Co and ^{63}Ni, have been computed within a complete microscopic fashion without assuming the Brink–Axel hypothesis for the analysis of GT strength in the excited states. The small difference is attributed to the usage of the Brink–Axel hypothesis and the incorporation of the quenching factor in the shell model calculation.

4 Conclusion

The RMF model has been utilized to analyze the nuclear structural properties, including PECs and deformation parameters for ^{63}Co and ^{63}Ni. The analysis was performed using the DD-ME2 interaction under the blocking technique. The RMF-based analysis predicted an oblate shape for ^{63}Co and a prolate shape for the ^{63}Ni in their ground states. The β_2 values computed via the RMF framework are later utilized as input parameters in the pn-QRPA model to perform the analysis of the GT strength and stellar weak rates. The calculated GT distributions were found to be in reasonable agreement with the measured data. The stellar weak-interaction rates for ^{63}Co and ^{63}Ni have been computed within a complete microscopic fashion without assuming the Brink–Axel hypothesis for the analysis of GT strength in the excited states. The pn-QRPA-based computed weak rates have been compared with the previously shell model-based computed rates. The reported weak rates are larger than the previous calculations by as much as a factor of 4. The difference is attributed to the usage of the Brink–Axel hypothesis and the incorporation of the quenching factor in the shell model calculation. The reported stellar rates could prove useful for *r*-process nucleosynthesis calculations and simulations of late-time stellar evolution.

Data availability statement

The raw data supporting the conclusions of this article will be made available by the authors, without undue reservation.

Author contributions

AK: conceptualization, investigation, software, supervision, writing–original draft, and writing–review and editing. J-UN: investigation and writing–original draft. HA: funding acquisition, project administration, software, and writing–review and editing. IA: data curation and writing–review and editing. N-UR: investigation and writing–review and editing.

Funding

The author(s) declare that financial support was received for the research, authorship, and/or publication of this article. This research was funded by Taif University, Saudi Arabia, Project No. TU-DSPP-2024-33.

Acknowledgments

The authors extend their appreciation to Taif University, Saudi Arabia, for supporting this work through project number (TU-DSPP-2024-33). Jameel-Un Nabi would like to acknowledge the support of Higher Education Commission Pakistan through the project number 20-15394/NRPU/R&D/HEC/2021.

Conflict of interest

The authors declare that the research was conducted in the absence of any commercial or financial relationships that could be construed as a potential conflict of interest.

Publisher's note

References

1. Burbidge EM, Burbidge GR, Fowler WA, Hoyle F. Synthesis of the elements in stars. *Rev Mod Phys* (1957) 29:547–650. doi:10.1103/RevModPhys.29.547

2. Coryell CD. The chemistry of creation of the heavy elements. *J Chem* (1961) 38:67. doi:10.1021/ed038p67

3. Kratz KL, Bitouzet JP, Thielemann FK, Moeller P, Pfeiffer B. Isotopic r-process abundances and nuclear structure far from stability - implications for the r-process mechanism. *Astrophys J* (1993) 403:216–38. doi:10.1086/172196

4. Usman S, Mushtaq A. Magnetorotational instability in dense electron-positron-ion plasmas. *Sci Rep* (2023) 13:15315. doi:10.1038/s41598-023-42397-3

5. Langanke K, Martínez-Pinedo G. Shell-model calculations of stellar weak interaction rates: II. Weak rates for nuclei in the mass range $A = 45 - -65$ in supernovae environments. *Nucl Phys A* (2000) 673:481–508. doi:10.1016/S0375-9474(00)00131-7

6. Fujita Y, Akimune H, Daito I, Fujimura H, Fujiwara M, Harakeh MN, et al. Mirror-symmetry structure of $A = 27$, $T = 1/2$ nuclei studied through strong, weak, and electromagnetic interactions. *Phys Rev* (1999) 59:90–100. doi:10.1103/PhysRevC.59.90

7. Cole AL, Akimune H, Austin SM, Bazin D, Berg AV, GPA B, et al. Measurement of the Gamow-Teller strength distribution in Co-58 via the Ni-58 (t, He-3) reaction at 115-MeV/nucleon. *Phys Rev C* (2006) 74:034333. doi:10.1103/PhysRevC.74.034333

8. Fujita Y, Rubio B, Gelletly W. Spin-isospin excitations probed by strong, weak and electro-magnetic interactions. *Prog Part Nucl Phys* (2011) 66:549–606. doi:10.1016/j.ppnp.2011.01.056

9. Avignone IIIFT, Elliott SR, Engel J. Double beta decay, Majorana neutrinos, and neutrino mass. *Rev Mod Phys* (2008) 80:481–516. doi:10.1103/RevModPhys.80.481

10. Wang LJ, Engel J, Yao JM. Quenching of nuclear matrix elements for $0\nu\beta\beta$ decay by chiral two-body currents. *Phys Rev C* (2018) 98:031301. doi:10.1103/PhysRevC.98.031301

11. Yao JM, Engel J, Wang LJ, Jiao CF, Hergert H. Generator-coordinate reference states for spectra and $0\nu\beta\beta$ decay in the in-medium similarity renormalization group. *Phys Rev* (2018) 98:054311. doi:10.1103/PhysRevC.98.054311

12. Fuller GM, Fowler WA, Newman MJ. Stellar weak-interaction rates for sd-shell nuclei. I-Nuclear matrix element systematics with application to Al-26 and selected nuclei of importance to the supernova problem. *Astrophys J Suppl Ser* (1980) 42:447. doi:10.1086/190657

13. Fuller GM, Fowler WA, Newman MJ. Stellar weak interaction rates for intermediate-mass nuclei. II-$A = 21$ to $A = 60$. *Astrophys J* (1982) 252:715. doi:10.1086/159597

14. Fuller GM, Fowler WA, Newman MJ. Stellar weak interaction rates for intermediate mass nuclei. III-Rate tables for the free nucleons and nuclei with $A = 21$ to $A = 60$. *Astrophys J Suppl Ser* (1982) 48:279. doi:10.1086/190779

15. Langanke K, Martínez-Pinedo G. Nuclear weak-interaction processes in stars. *Rev Mod Phy* (2003) 75:819–62. doi:10.1103/RevModPhys.75.819

16. Martínez-Pinedo G, Lam YH, Langanke K, Zegers RGT, Sullivan C. Astrophysical weak-interaction rates for selected $A = 20$ and $A = 24$ nuclei. *Phys Rev* (2014) 89:045806. doi:10.1103/PhysRevC.89.045806

17. Langanke K, Martínez-Pinedo G, Zegers RGT. Electron capture in stars. *Rep Prog Phys* (2021) 84:066301. doi:10.1088/1361-6633/abf207

18. Janka H-T, Langanke K, Marek A, Martínez-Pinedo G, Müller B. Theory of core-collapse supernovae. *Phys Rep* (2007) 442:38–74. doi:10.1016/j.physrep.2007.02.002

19. Käppeler F, Gallino R, Bisterzo S, Aoki W. The s process: nuclear physics, stellar models, and observations. *Rev Mod Phys* (2013) 83:157–93. doi:10.1103/RevModPhys.83.157

20. Kabir A, Abideen ZU, Nabi J-U. Re-Investigation of neutron capture by ^{84}Kr and ^{86}Kr in the s-process nucleosynthesis. *Braz J Phys* (2024) 54:8. doi:10.1007/s13538-024-01455-5

21. Cowan JJ, Sneden C, Lawler JE, Aprahamian A, Wiescher M, Langanke K, et al. Origin of the heaviest elements: the rapid neutron-capture process. *Rev Mod Phys* (2021) 93:015002. doi:10.1103/RevModPhys.93.015002

22. Schatz H, Aprahamian A, Görres J, Wiescher M, Rauscher T, Rembges JF, et al. rp-Process nucleosynthesis at extreme temperature and density conditions. *Phys Rep* (1998) 294:167–263. doi:10.1016/s0370-1573(97)00048-3

23. Cole AL, Anderson TS, Zegers RGT, Austin SM, Brown BA, Valdez L, et al. Gamow-Teller strengths and electron-capture rates for pf-shell nuclei of relevance for late stellar evolution. *Phys Rev* (2012) 86:015809. doi:10.1103/PhysRevC.86.015809

24. Langanke K, Martínez-Pinedo G, Sampaio JM, Dean DJ, Hix WR, Messer OEB, et al. Electron capture rates on nuclei and implications for stellar core collapse. *Phys Rev Lett* (2003) 90:241102. doi:10.1103/PhysRevLett.90.241102

25. Ejiri H, Suhonen J, Zuber K. Neutrino-nuclear responses for astro-neutrinos, single beta decays and double beta decays. *Phys Rep* (2019) 797:1–102. doi:10.1016/j.physrep.2018.12.001

26. Sun Y, Feng DH. High spin spectroscopy with the projected shell model. *Phys Rep* (1996) 264:375–91. doi:10.1016/0370-1573(95)00049-6

27. Chen ZR, Wang LJ. Stellar β^- decay rates for ^{63}Co and ^{63}Ni by the projected shell model. *Symmetry* (2023) 15:315. doi:10.3390/sym15020315

28. Heger A, Langanke K, Martínez-Pinedo G, Woosley SE. Presupernova collapse models with improved weak-interaction rates. *Phys Rev Lett* (2001) 86:1678–81. doi:10.1103/PhysRevLett.86.1678

29. Ring P. Relativistic mean field theory in finite nuclei. *Prog Part Nucl Phys* (1996) 37:193–263. doi:10.1016/0146-6410(96)00054-3

30. Walecka JD. A theory of highly condensed matter. *Ann Phys* (1974) 83:491–529. doi:10.1016/0003-4916(74)90208-5

31. Nikšić T, Vretenar D, Ring P. Relativistic nuclear energy density functionals: adjusting parameters to binding energies. *Phys Rev C* (2008) 78:034318. doi:10.1103/PhysRevC.78.034318

32. Lalazissis GA, Nikšić T, Vretenar D, Ring P. New relativistic mean-field interaction with density-dependent meson-nucleon couplings. *Phys Rev* (2005) 71:024312. doi:10.1103/PhysRevC.71.024312

33. Typel S, Wolter HH. Relativistic mean field calculations with density-dependent meson-nucleon coupling. *Nucl Phys A* (1999) 656:331–64. doi:10.1016/S0375-9474(99)00310-3

34. Meng J, Toki H, Zhou SG, Zhang SQ, Long WH, Geng LS. Relativistic continuum Hartree Bogoliubov theory for ground-state properties of exotic nuclei. *Prog Part Nucl Phys* (2006) 57:470–563. doi:10.1016/j.ppnp.2005.06.001

35. Nikšić T, Vretenar D, Finelli P, Ring P. Relativistic Hartree-Bogoliubov model with density-dependent meson-nucleon couplings. *Phys Rev* (2002) 66:024306. doi:10.1103/PhysRevC.66.024306

36. Nabi JU, Kabir A, Khalid W, Rida SA, Anwaar I. Investigation of nuclear structure and β-decay properties of as isotopes. *Chin J Phys* (2024) 92:22–32. doi:10.1016/j.cjph.2024.08.037

37. Nabi JU, Kabir A, Bayram T. Re-analysis of the Gamow-Teller distributions for $N = Z$ nuclei, ^{24}Mg, ^{28}Si, and ^{32}S. *Chin J Phys* (2024) 87:797–803. doi:10.1016/j.cjph.2023.12.036

38. Nabi JU, Khalid W, Kabir A, Rida SA. Study of β-decay, log ft values and nuclear structure properties of neutron-rich Ge nuclei. *Arab J Sci Eng* (2024) 1–13. doi:10.1007/s13369-024-09619-w

39. Ring P, Schuck P. *The nuclear many-body problem*. Springer Science and Business Media (2004).

40. Stoitsov MV, Dobaczewski J, Nazarewicz W, Ring P. Axially deformed solution of the Skyrme-Hartree-Fock-Bogolyubov equations using the transformed harmonic oscillator basis. The program HFBTHO (v1.66p). *Comp Phys Commu* (2005) 167:43–63. doi:10.1016/j.cpc.2005.01.001

41. Nikšić T, Paar N, Vretenar D, Ring P. DIRHB-A relativistic self-consistent mean-field framework for atomic nuclei. *Comp Phys Commu* (2014) 185:1808–21. doi:10.1016/j.cpc.2014.02.027

42. Nilsson SG. Binding states of individual nucleons in strongly deformed nuclei. *Dan Mat Fys Medd* (1955) 29:1–69.

43. Ragnarsson I, Sheline RK. Systematics of nuclear deformations. *Phys Scr* (1984) 29:385–401. doi:10.1088/0031-8949/29/5/001

44. Kondev FG, Wang M, Huang WJ, Naimi S, Audi G. The NUBASE2020 evaluation of nuclear physics properties. *Chin Phys C* (2021) 45:030001. doi:10.1088/1674-1137/abddae

45. Möller P, Sierk AJ, Ichikawa T, Sagawa H. Nuclear ground-state masses and deformations: FRDM. *Data Nucl Data Tables* (2012) 109:1–204. doi:10.1016/j.adt.2015.10.002

46. Muto K, Bender E, Klapdor HV. Proton-neutron quasiparticle RPA and charge-changing transitions. *Z Phys A Atom Nuclei* (1989) 333:125–9. doi:10.1007/BF01565141

47. Homma H, Bender E, Hirsch M, Muto K, Klapdor-Kleingrothaus HV, Oda T. Systematic study of nuclear β decay. *Phys Rev* (1996) 54:2972–85. doi:10.1103/PhysRevC.54.2972

48. Ikeda K, Fujii S, Fujita JI. The reactions and beta decays. *Phys Lett* (1963) 3:271–2. doi:10.1016/0031-9163(63)90255-5

49. Staudt A, Bender E, Muto K, Klapdor-Kleingrothaus HV. Second-generation microscopic predictions of beta-decay half-lives of neutron-rich nuclei. *Data Nucl Data Tables* (1990) 44:79–132. doi:10.1016/0092-640X(90)90020-K

50. Hirsch M, Staudt A, Klapdor-Kleingrothaus HV. Prediction of average β and γ energies and probabilities of β-delayed neutron emission in the region of fission products. *Data Nucl Data Tables* (1992) 51:243–71. doi:10.1016/0092-640X(92)90002-Y

51. Muto K, Bender E, Oda T, Klapdor-Kleingrothaus HV. Proton-neutron quasiparticle RPA with separable Gamow-Teller forces. *Z Phys A Hadrons Nuclei* (1992) 341:407–15. doi:10.1007/BF01301384

52. Gove NB, Martin MJ. Log-f tables for beta decay. *Data Nucl Data Tables* (1971) 10:205–19. doi:10.1016/S0092-640X(71)80026-8

53. phynu (2024). Available from: https://www-phynu.cea.fr/science_en_ligne/carte_potentiels_microscopiques/noyaux/zz28/zz28nn36all_eng.html (Accessed June 29, 2024).

54. nndc (2024). Available from: https://www.nndc.bnl.gov (Accessed June 29, 2024).